JOURNAL OF CATALYSIS 97, 121–136 (1986)

Fischer–Tropsch Synthesis over Reduced and Unreduced Iron Oxide Catalysts

RONALD A. DICTOR[1] AND ALEXIS T. BELL

Materials and Molecular Research Division, Lawrence Berkeley Laboratory, and Department of Chemical Engineering, University of California, Berkeley, California 94720

Received February 26, 1985; revised August 19, 1985

An investigation has been carried out of Fischer–Tropsch synthesis over potassium-promoted and unpromoted iron oxide catalysts. The distribution of products over reduced and unreduced Fe_2O_3 are similar. The primary products are methane and linear, terminal olefins. Some C_2^+ paraffins are produced in parallel with olefins, but most result from hydrogenation of the olefins. Isomerization of terminal to internal olefins also occurs as a secondary reaction. The Anderson–Schulz–Flory distribution of products is characterized by two branches differing in the value of α. The average molecular weight of the product increases with decreasing temperature, decreasing H_2 partial pressure, and increasing CO partial pressure. Methanol is the only oxygenated product formed over unpromoted Fe_2O_3. Promotion of Fe_2O_3 with potassium suppresses the rates of olefin hydrogenation and isomerization, and the rate of methanol formation, but enhances the rates of formation of C_2^+ hydrocarbons, branched hydrocarbons, and aldehydes. The kinetics for the synthesis of C_1–C_7 hydrocarbons were determined for both promoted and unpromoted catalysts. The data show that in general the kinetics of formation of an individual product cannot be represented by simple power-law rate expressions. Based on X-ray diffraction analyses of used catalysts, it is concluded that the phase of iron active for Fe_2O_3 Fischer–Tropsch synthesis is a mixture of χ- and ε'-iron carbides, and a small amount of α-iron.

INTRODUCTION

While iron-based catalysts for Fischer–Tropsch synthesis have been known for over 60 years (*1–3*), a controversy still exists regarding the composition of the catalytically active phase of iron. The difficulty arises from the fact that under reaction conditions, iron can exist as magnetite, α-iron, or one of several iron carbides, and that the distribution of these phases is a sensitive function of reaction conditions and time under reaction conditions. Bonzel and coworkers (*4–7*) and Dwyer and co-workers (*8, 9*) have shown that while α-iron is quite active for Fischer–Tropsch, it rapidly deactivates due to formation of a graphitic overlayer. Raupp and Delgass (*10*) have proposed that iron carbide is needed to achieve high activity since they observed that the increase in activity of an iron catalyst with time under reaction conditions paralleled the accumulation of iron carbide. A similar correlation has been reported by Niemantsverdriet *et al.* (*11*). More recently, Teichner and co-workers (*12–14*) have proposed that Fe_3O_4 is an active catalyst for hydrocarbon synthesis and unlike metallic iron does not form an inactive iron carbide or carbon overlayers which can contribute to catalyst deactivation.

The present study was undertaken as part of an investigation to identify the influence of catalyst composition on the performance of iron-based Fischer–Tropsch catalysts for synthesis. We report here results obtained with reduced and unreduced Fe_2O_3, and with unreduced, potassium-promoted Fe_2O_3. All of the experiments were carried out in a well-stirred autoclave reactor containing a slurry of the catalyst in

[1] Present address: General Motors Research Laboratories, Warren, Mich. 48090.

0021-9517/86 $3.00

molten paraffin wax. The kinetics of Fischer–Tropsch synthesis were measured over a broad range of reaction conditions. The composition of the used catalyst was determined by X-ray diffraction.

EXPERIMENTAL

Materials

Hematite, Fe_2O_3, was obtained from Alfa Products. The oxide consists of particles with diameters between 1 and 5 μm (BET surface area = 9.0 m^2/g). Potassium-promoted Fe_2O_3, referred to hereafter as K/Fe_2O_3, was prepared by adding Fe_2O_3 to a solution of K_2CO_3 in deionized water and then drying the resultant slurry. The atomic K/Fe ratio of the dried material was 0.011.

The medium used to suspend the catalyst was molten Amoco Parowax (melting point $\simeq$ 60°C), a mixture of C_{20}–C_{45} linear paraffins. The wax also contains trace amounts of C_{16}–C_{19} paraffins.

Apparatus

Reactions were carried out in a 450-cm^3 Parr minireactor equipped with two 1.5-in. impellers to stir the liquid phase and one 1.0-in. propeller to stir the gas in the head space. The reactor temperature was maintained using a heating mantle operated through a proportional temperature controller. H_2 and CO were fed to the reactor through high-pressure flow controllers. The reactor effluent was passed through heat-traced stainless-steel lines to two traps connected in series. The first trap was kept at 25°C, and the second trap was maintained at 0°C in an ice-water bath. The noncondensable gases were passed through a back-pressure regulator and then vented.

Details of the analytical system have been presented elsewhere (*15*). Products containing 1 to 30 carbon atoms were analyzed on line by gas chromatography. To do this, a portion of the reactor effluent was bled through a high-temperature metering valve, passed through a 7-μm in-line filter, and sampled periodically using a heated sampling valve. Separation of the products was achieved with a 50-m capillary column coated with 0V-101. For an analysis of the light products (CO_2, C_1–C_5 hydrocarbons, and C_1–C_3 oxygenates) a bleed from the effluent was passed through a water-cooled heat exchanger and then through a sampling valve. Separation of the light gases was achieved with a 2.4-m column packed with Porapak Q. The products eluting from the capillary column were detected with a FID and those from the packed column with a TCD.

Approximately 5–10 g of catalyst and 160 g of wax were used for the experiments reported here. The wax was first melted in the open reactor. Then, the catalyst was added, and the reactor was sealed and attached to the flow system. The reactor was purged with flowing helium for 10–15 min as the temperature was raised to 100–120°C. The helium was then replaced with CO and H_2, and the pressure was raised from 1 to 8 atm. Following the introduction of reactant gases, the temperature was set for 250°C, which was reached after 20–30 min. For some of the experiments the catalyst was reduced prior to introduction of the synthesis mixture. Reduction was carried out at 300°C for 20 h in 10 atm of flowing H_2.

Accumulation of heavy products in the molten wax prevented the system from ever fully reaching steady-state operation. To obtain representative rates of formation of C_1–C_{16} products, it was necessary to operate the reactor at a fixed set of conditions for 1–2 days. Much shorter periods of operation (2–4 h) were used if interest focused only on C_1–C_7 products. For all of the conditions studied, the flow rate of syngas was maintained sufficiently high to keep the CO conversion below 5%.

Catalyst Activity

Figures 1–3 show plots of catalyst activity as a function of time on stream for reduced Fe_2O_3, unreduced Fe_2O_3, and K/Fe_2O_3. Hydrocarbon synthesis activity is expressed as the rate at which carbon ap-

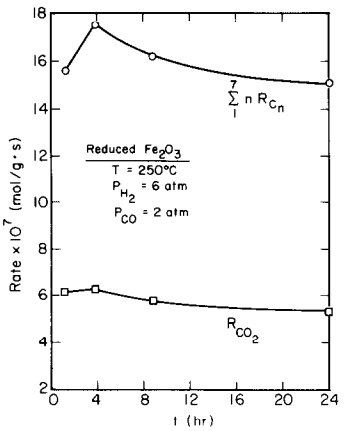

FIG. 1. Catalytic activity of prereduced Fe_2O_3 following introduction of CO at 250°C. The catalyst was reduced for 20 h in 10 atm H_2.

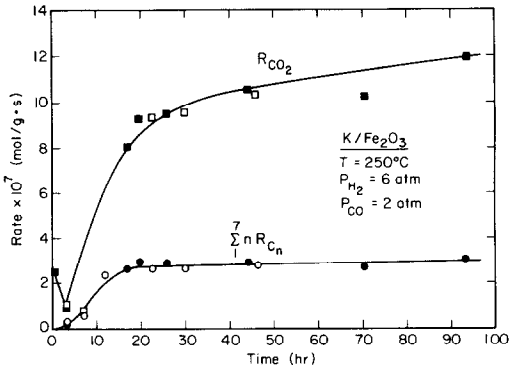

FIG. 3. Activity for potassium-promoted Fe_2O_3 following reactor start-up. Hydrocarbon activity is represented as the rate at which carbon appears in C_1–C_7 hydrocarbon products.

pears in C_1 through C_7 hydrocarbons. This rate accounts for more than 75% of the total carbon appearing in hydrocarbons. The rate of CO_2 formation is also shown as a function of time for each case. For reduced Fe_2O_3 (Fig. 1) the synthesis rate rises during the first 4 h under reaction conditions and then declines monotonically thereafter. The rate of CO_2 formation follows a similar but less pronounced trend. The change in synthesis activity with time on stream is similar for Fe_2O_3 and K/Fe_2O_3. There is an initial induction period after which the activity rises rapidly. The induction period for Fe_2O_3 (see Fig. 2) is 10–15 h while that for K/Fe_2O_3 (see Fig. 3) is approximately 10 h of exposure to synthesis gas. The rate of CO_2 formation for both unreduced catalysts is high initially, but then decreases during the hydrocarbon-synthesis induction period. Following this, the rate of CO_2 formation increases in a manner paralleling the increase in synthesis activity. The rates of hydrocarbon synthesis and CO_2 formation observed after 160 h with unreduced Fe_2O_3 are comparable to those observed after 4 h with reduced Fe_2O_3. On the other hand, the steady-state synthesis activity of unreduced K/Fe_2O_3 is nearly an order of magnitude lower than the maximum synthesis activity of unreduced Fe_2O_3, and the maximum rate of CO_2 formation for unreduced K/Fe_2O_3 is twice as high as that for unreduced Fe_2O_3.

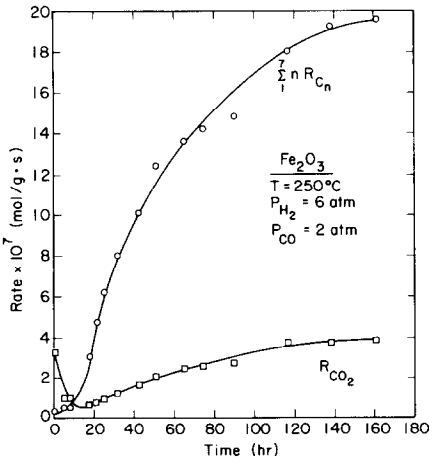

FIG. 2. Activity for Fe_2O_3 following reactor start-up. Hydrocarbon activity is represented as the rate at which carbon appears in C_1–C_7 hydrocarbon products.

Product Distribution

The principal products formed during Fischer–Tropsch synthesis over unpromoted Fe_2O_3 are *n*-olefins, *n*-paraffins, methanol, carbon dioxide, and water. Methanol is the only oxygenated product present in significant concentration. No evidence was found for branched products. It is impor-

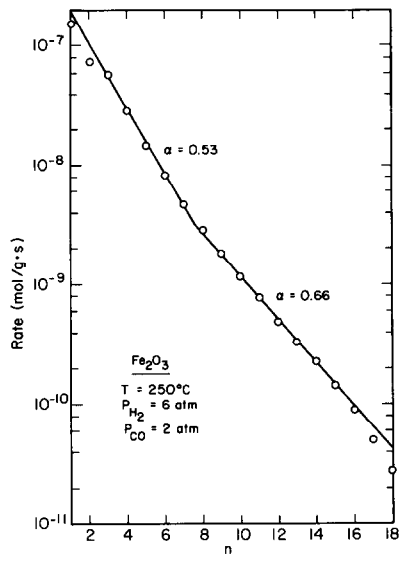

FIG. 4. Hydrocarbon product distribution observed using Fe_2O_3. Each point represents the sum of the rates of all linear olefins and paraffins of the same carbon number.

tant to emphasize that virtually identical product distribution were obtained with prereduced and unreduced Fe_2O_3. In view of this, only the data for unreduced Fe_2O_3 will be presented below.

The hydrocarbon product distribution is illustrated in Fig. 4 in the form of an Anderson–Schulz–Flory plot, a semilogarithmic plot of reaction rate versus the number of carbons in the product, n. The observed distribution can be described by two straight-line segments: one for C_1–C_9 hydrocarbons characterized by $\alpha = 0.53$ and the second for C_{10}–C_{15} hydrocarbons characterized by $\alpha = 0.66$. The deviation of C_{15}^+ products from the second line segment is due to the hold-up of these components in the slurry and/or the transfer lines from the reactor to the analytical system (*16*). No change in the distribution of products was observed with increasing time under reaction conditions.

The effects of reaction conditions on α for C_1 through C_9 hydrocarbons are presented in Table 1. The value of α increases noticeably with decreasing H_2 partial pressure, increasing CO partial pressure, and decreasing temperature. Gas velocity, however, has no effect on α.

The effects of reactant partial pressures, temperature, and gas flow rate on 1-olefin selectivity was carefully investigated. Figure 5 is illustrative of the data obtained for C_2 through C_{15} 1-olefins. The selectivity has a maximum at $n = 3$ and then drops precipitously for heavier hydrocarbons. For a fixed carbon number, the 1-olefin selectivity was observed to increase with decreasing H_2 partial pressure, increasing CO par-

TABLE 1

Values of α for Fe_2O_3 and K/Fe_2O_3

Operating conditions			α
		Fe_2O_3	
T = 212°C, P_{H_2} = 4 atm	P_{CO}	1 atm	0.58
		2 atm	0.64
		4 atm	0.66
		8 atm	0.67
T = 213°C, P_{CO} = 2 atm	P_{H_2}	1 atm	0.70
		2 atm	0.72
		4 atm	0.63
		8 atm	0.58
P_{CO} = 2 atm, P_{H_2} = 6 atm	T	241°C	0.59
		223	0.63
		214	0.60
		199	0.64
		188	0.68
T = 242°C, P_{CO} = 2 atm, P_{H_2} = 2 atm	G	900 cm³/min	0.67
		400 cm³/min	0.67
		200 cm³/min	0.67
		K/Fe_2O_3	
T = 240°C, P_{H_2} = 5 atm	P_{CO}	1 atm	0.68
		2 atm	0.68
		4 atm	0.69
		8 atm	0.70
T = 240°C, P_{CO} = 2 atm	P_{H_2}	1 atm	0.71
		2 atm	0.69
		4 atm	0.68
		8 atm	0.66
P_{CO} = 2 atm, P_{H_2} = 6 atm	T	261°C	0.66
		251	0.66
		237	0.66
		224	0.69
		211	0.68
T = 249°C, P_{CO} = 3 atm, P_{H_2} = 3 atm	G	960 cm³/min	0.69
		500 cm³/min	0.68
		200 cm³/min	0.70

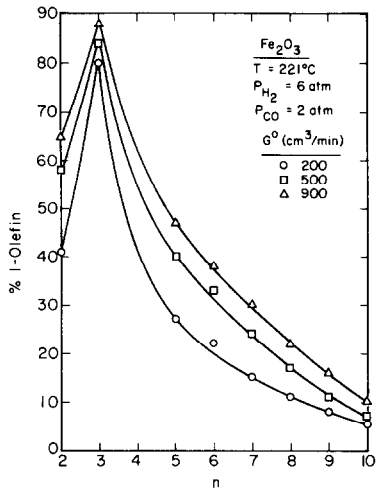

FIG. 5. Selectivity for 1-olefins as a function of inlet gas velocity. Selectivity is defined as percentage of 1-olefins in total hydrocarbon product of the same carbon.

tial pressure, and decreasing temperature. As seen in Fig. 5, the 1-olefin selectivity increases with increasing gas flow rate demonstrating that 1-olefins are primary products that can react through secondary processes to form paraffins and internal olefins. It was observed, though, that even at the highest gas flow rate the propylene selectivity never exceeded 90%, suggesting that paraffins may be formed as both primary and secondary products.

The influence of reaction conditions on the production of internal olefins was also investigated, and an illustration of the results is presented in Fig. 6. In this plot, internal olefin selectivity is calculated using the rate of production of internal olefins as a percentage of the total of the production rates for all olefins for each carbon number. Figure 6 shows that internal olefin selectivity increases with carbon number. This is largely due to the longer residence times for heavier products in the reactor. Higher molecular weight products have a greater probability of undergoing secondary processes than lighter products since the higher solubility of these products increases their content in the liquid phase. Part of this trend may also be due to differences in the reactivity among products, as similar results for olefin selectivity are observed by Schulz *et al.* (*17*) and Schulz and Gökcebay (*18*) using a fixed-bed reactor. The formation of internal olefins occurs to a greater extent at high H_2 pressures and low CO pressures. Both of these trends are consistent with the results presented above for 1-olefin selectivity. Increasing the temperature increases the rates of olefin isomerization but not very significantly. This may be due in part to the decrease in the concentration of primary olefins caused by the decrease in olefin solubility with increasing temperature.

The promotion of Fe_2O_3 with potassium results in a number of modifications in the product distribution. Olefin hydrogenation and isomerization are suppressed, and the formation of aldehydes and branched hydrocarbons are enhanced. On the other hand, the formation of methanol is reduced by the presence of potassium. The distribution of hydrocarbon products (*n*-alkanes + linear-olefins) formed over K/Fe_2O_3 is illustrated in Fig. 7. As for Fe_2O_3, the distribution can be described by two linear branches—one for C_1–C_7 hydrocarbons characterized by $\alpha = 0.66$ and one for C_8–C_{15} hydrocarbons characterized by $\alpha = 0.86$. Comparison of Figs. 4 and 7 shows

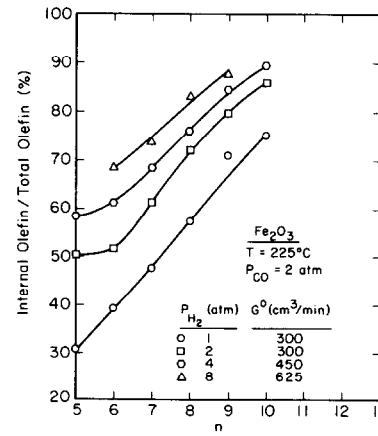

FIG. 6. Influence of H_2 partial pressure on the selectivity for internal olefins.

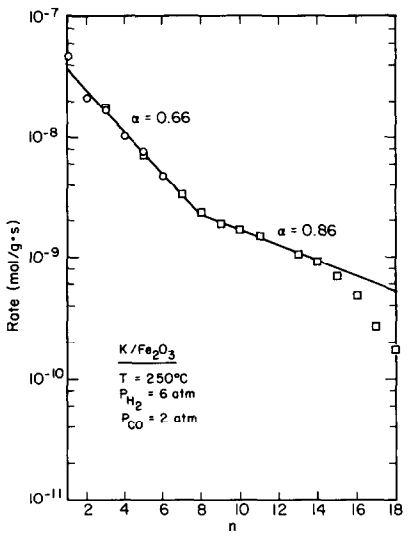

FIG. 7. Hydrocarbon product distribution observed using potassium-promoted Fe_2O_3. Each point represents the sum of the rates of all linear olefins and paraffins of the same carbon number.

that both α values are greater for K/Fe_2O_3 than for Fe_2O_3. It is also noted that while potassium promotion reduces the absolute rates of production of C_1–C_7 hydrocarbons, the rates of production of C_8–C_{15} hydrocarbons are increased.

The effects of reaction conditions on α for C_1–C_7 hydrocarbons are presented in Table 1. The changes in α with H_2 and CO partial pressures, and temperature, for K/Fe_2O_3 are qualitatively similar to those for Fe_2O_3 but much smaller in magnitude.

The influence of reaction conditions on the percentage of 1-olefins formed over K/Fe_2O_3 was investigated, and an illustration of the results is presented in Fig. 8. In all cases (except $n = 3$) the proportion of 1-olefins formed over K/Fe_2O_3 is significantly higher than that formed over unpromoted Fe_2O_3. The rate at which the olefin selectivity decreases with increasing carbon number is much lower for K/Fe_2O_3. In agreement with the behavior of Fe_2O_3, the percentage of olefins decreases with increasing H_2 partial pressure. Potassium promotion, however, alters the effects of CO partial pressure, gas velocity, and temperature. CO partial pressure and synthesis gas flow rate have little, if any, effect. On the other hand, the olefin selectivity increases with increasing temperature, which is exactly opposite the pattern seen for unpromoted Fe_2O_3.

For most reaction conditions, the concentrations of internal olefins in the products were so small that they could not be measured accurately. It was observed though that as with unpromoted Fe_2O_3, the proportion of internal olefins increased with carbon number, and was greatest for high H_2 partial pressures and low CO partial pressures. Quantitative determination of the internal olefin content was made for a temperature of 250°C, and H_2 and CO partial pressures of 6 and 0.5 atm, respectively. In this case, the percentage of internal olefins rises from 2% for $n = 5$ to 15% for $n = 14$.

Branched products are formed in significant quantities over K/Fe_2O_3 in a strong contrast to what was observed for unpromoted Fe_2O_3. The predominant branched products are methyl-branched olefins. No clearly discernible trends are observed in branched product yields as functions of P_{H_2}, P_{CO}, and temperature. The rate of 4-methyl-1-pentene formation is typically ~10% that of the straight-chain C_6 products, and the total yield of branched products does not exceed 20% of all hydrocar-

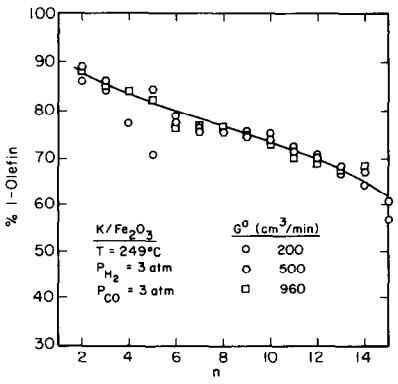

FIG. 8. Selectivity for 1-olefins as a function of inlet gas velocity. Selectivity is defined as percentage of 1-olefins in total of linear hydrocarbons.

bons. No definitive relationship could be observed between the extent of branching and carbon number, due to the decline in chromatographic resolution of peaks with increasing molecular weight (*15*).

An example of the distribution of aldehydes as a function of carbon number is presented in Fig. 9, along with the distribution of hydrocarbons from the same sample. Because it is believed that aldehydes are formed by CO insertion into a growing surface alkyl group (*19, 20*) and subsequent reductive elimination of the acyl group, the aldehyde data are plotted versus $n - 1$ as one carbon is acquired in the termination step. Termination for hydrocarbons, on the other hand, is thought to occur by elimination of a hydrogen atom from an alkyl group to form an olefin. While the chromatographic data for aldehydes are more difficult to acquire because of low concentrations and peak overlap, it appears that, within experimental uncertainty, the distribution of aldehydes parallels that of the hydrocarbons.

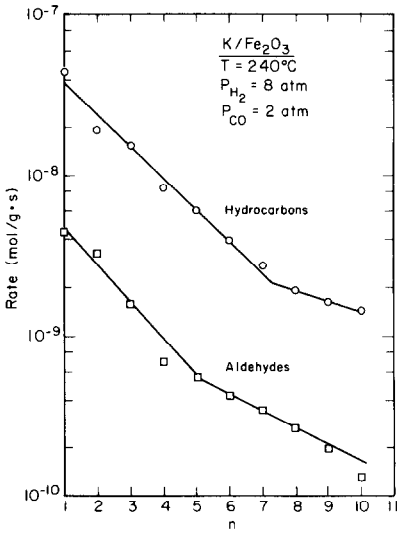

FIG. 9. Distribution of hydrocarbons and aldehydes from a common effluent sample. Each point for hydrocarbons represents the sum of 1-olefin plus *n*-paraffin; only straight-chain aldehydes are measured.

Kinetics

The dependence of the rates of C_1–C_7 hydrocarbon synthesis on temperature and H_2 and CO partial pressures were investigated for both Fe_2O_3 and K/Fe_2O_3. In analyzing the data, the rates of olefin and paraffin production were lumped together. This procedure is justified only for systems in which paraffins are formed exclusively by sequential hydrogenation of olefins, and olefins do not undergo reactions which cause a change in carbon number. Satterfield *et al.* (*21*) and Cannella and Bell (*22*) have shown that incorporation of olefins into growing alkyl chains is negligible over iron catalysts. For Fischer–Tropsch synthesis over Fe_2O_3, combination of olefins and paraffins is justified because paraffins are formed largely by hydrogenation of olefins. For K/Fe_2O_3 paraffins are formed almost exclusively by a pathway which parallels the formation of olefins. However, since the proportion of paraffins is small lumping of

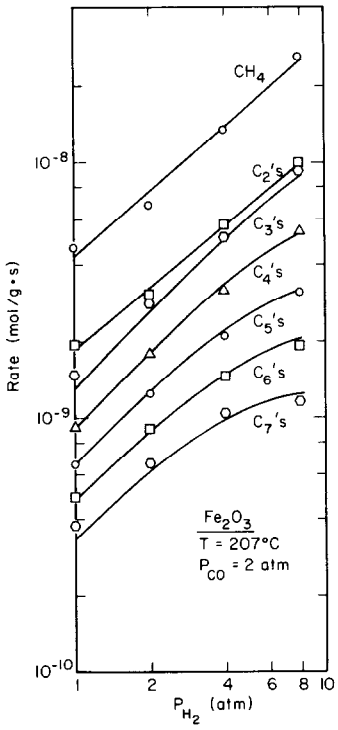

FIG. 10. Rates of production of light hydrocarbons over Fe_2O_3 as a function of H_2 partial pressure. Each point represents the sum of the rates of all hydrocarbons with the same carbon number. The curves for n = 1 and 2 are hand drawn; those for n = 3 to 7 are based on Eqs. (3) and (6) of the text.

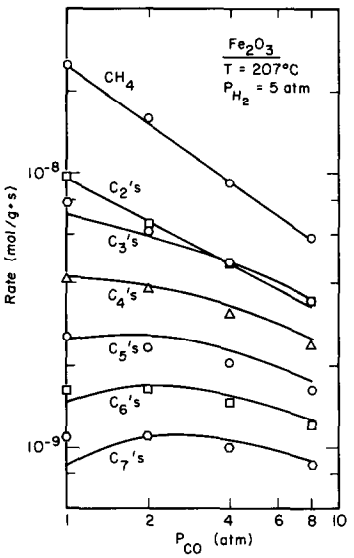

FIG. 11. Rates of production of light hydrocarbons over Fe_2O_3 as a function of CO partial pressure. Each point represents the sum of the rates of all hydrocarbons with the same carbon number. The curves for n = 1 and 2 are hand drawn; those for n = 3 to 7 are based on Eqs. (3) and (6) of the text.

the data for olefins and paraffins does not lead to significant distortions.

Figures 10 and 11 show the dependence of the rates of formation of C_1–C_7 hydrocarbons over unreduced Fe_2O_3 on the partial pressures of H_2 and CO, respectively. Identical data were obtained for reduced Fe_2O_3 but are not shown since the results are virtually identical to those presented in Figs. 10 and 11. The data for C_1–C_3 hydrocarbons describe straight lines in Fig. 10, which suggests that the dependence of the rates of formation of these products on P_{H_2} can be described by a power law rate expression. As the carbon number increases beyond 3, the data become increasingly nonlinear. For the higher molecular weight products the dependence of rate on H_2 partial pressure diminishes with increasing H_2 partial pressure. The net effect is a decrease in H_2 dependence with increasing product molecular weight, a trend which is consistent with that for α reported in Table 1.

The dependences of the reaction rates on CO partial pressure shown in Fig. 11 are similar to those shown in Fig. 10 in that the synthesis rates of C_1 and C_2 products can be described by power-law expressions, whereas the rates of formation of the heavier products show increasing curvature with increasing n. While the CO dependence of methane is -0.75, the effective reaction order rapidly increases with carbon number. This trend is also reflected in the behavior of α reported in Table 1. It is interesting to note that the reaction rates of the higher hydrocarbons actually pass through maxima as the CO partial pressure increases from 0.5 to 8 atm.

Figures 12 and 13 are plots of reaction rates versus reactant partial pressures for synthesis over K/Fe_2O_3. The most significant difference between these figures and Figs. 10 and 11 is that all the data in Figs. 12 and 13 plot as straight lines. As a consequence, the rates of formation of each product over K/Fe_2O_3 can be described by a power-law rate expression in H_2 and CO

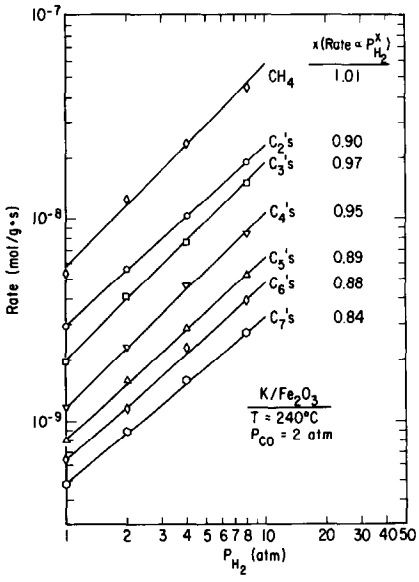

FIG. 12. Rates of production of light hydrocarbons over potassium-promoted Fe_2O_3 as a function of H_2 partial pressure. Each point represents the sum of the rates of 1-olefin plus n-paraffin. Lines are best-fit linear correlations.

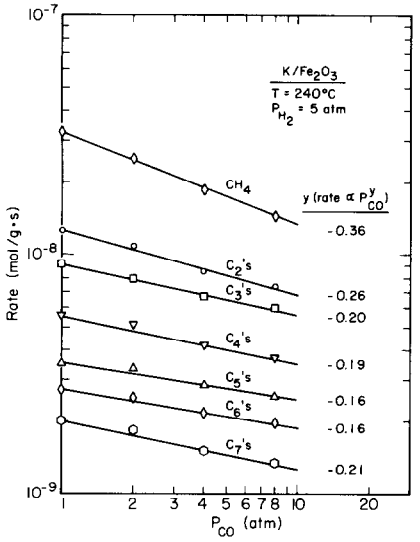

FIG. 13. Rates of production of light hydrocarbons over potassium-promoted Fe_2O_3 as a function of CO partial pressure. Each point represents the sum of the rates of 1-olefin plus *n*-paraffin. Lines are best-fit linear correlations.

partial pressures. The effective reaction order with respect to H_2 is near unity and decreases somewhat with increasing molecular weight. The order with respect to CO is approximately -0.4 for CH_4 and increases slightly with increasing molecular weight. The trends with increasing carbon number are much weaker for K/Fe_2O_3 than for Fe_2O_3, and this, in turn, accounts for the weaker dependence of α on P_{H_2} and P_{CO} for K/Fe_2O_3, shown in Table 1. When the data for olefins and paraffins are analyzed separately, it is found that the rate dependences on P_{CO} are the same but the reaction orders with respect to P_{H_2} are 0.2 to 0.4 greater for paraffins than olefins. This accounts for the observed decrease in olefin selectivity with increasing H_2 partial pressure.

Arrhenius plots for C_1–C_9 synthesis over Fe_2O_3 are shown in Fig. 14. The data for C_1–C_5 reaction lie along nearly parallel straight lines. The slope of these lines give an apparent activation energy, uncorrected for reactant solubility in the slurry, of approximately 26 kcal/mol. The data for C_6^+ hydrocarbons show increasing curvature with increasing molecular weight, and the effective activation energy, calculated using linear approximations of the data, decreases with increasing *n*. The deviation from linearity is not observed when the H_2 partial pressure is increased to 6 atm, but the activation energies still appear to decrease with increasing molecular weight. Consistent with this, the data in Table 1 show that α decreases with increasing temperature.

The Arrhenius plots for synthesis over K/Fe_2O_3 are linear and nearly parallel for all products in the C_1–C_9 range. The apparent activation energy determined from these plots is approximately 25 kcal/mol. Examination of the Arrhenius plots for olefins and paraffins reveals that the activation energies for olefins are 1–4 kcal/mol greater than for paraffins. The values of α for K/Fe_2O_3 are nearly invariant with temperature.

The rate of production of methanol over Fe_2O_3 is presented in Fig. 15 as functions of both H_2 and CO partial pressures. The rate exhibits an inverse dependence on H_2 par-

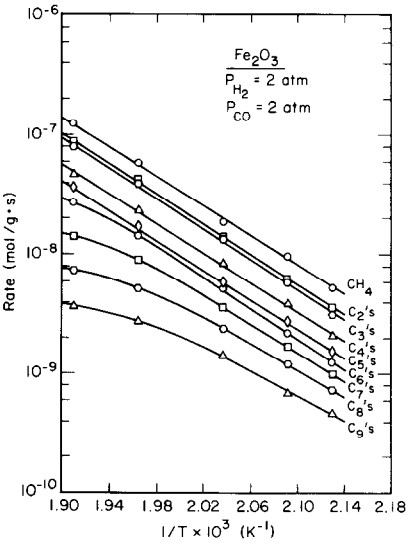

FIG. 14. Arrhenius plot for light hydrocarbons produced over Fe_2O_3. Each point is the sum of the rates of all hydrocarbons with the same carbon number.

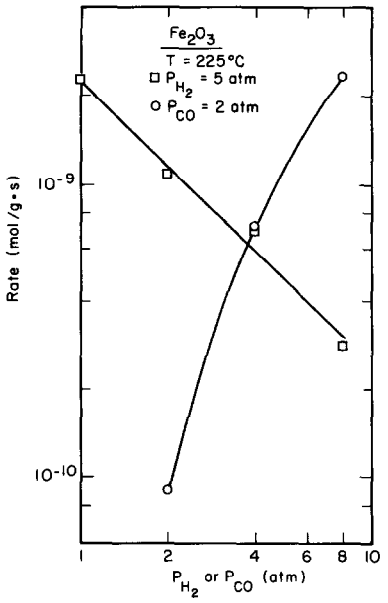

FIG. 15. Rate of methanol production as a function of reactant partial pressures.

tial pressure for $P_{H_2} < 4$ atm but decreases slightly at higher pressures. The apparent activation energy for this reaction, uncorrected for reactant solubilities in the slurry, is found to be 35.8 kcal/mol.

The rates of acetaldehyde formation over K/Fe_2O_3 are presented in Fig. 16 as functions of reactant partial pressures. The CO dependence of the rate is nearly zero order whereas the reaction order in H_2 is approximately 0.87. The apparent activation energy is 23.5 kcal/mol.

Characterization of Used Catalysts

Following each run, the catalyst was recovered from the slurry by first allowing the solids to settle in the melted wax and then rinsing solidified sections of the wax containing the catalyst in a Soxhlet extractor with isooctane. The cleaned samples were gently heated and later cooled under nitrogen to remove isooctane. X-Ray diffraction patterns of the dried catalyst were taken with a Siemens Model D500 diffractometer, using Cu$K\alpha$ radiation. The observed diffraction patterns for used unreduced Fe_2O_3 and K/Fe_2O_3, and reduced Fe_2O_3 are shown in Fig. 17. The peak positions noted in this figure are listed in Table 2, and are assigned to specific phases. Magnetite, Fe_3O_4, is the dominant iron phase observed in the used samples of unreduced Fe_2O_3 and K/Fe_2O_3. Peaks characteristic of Hägg (or χ) carbide are clearly evident and there appears to be a small amount of ε-carbide as well. Small amounts of α-Fe may also be present since a peak at 1.17 Å (not shown in Fig. 18) is often observed. Comparison of the patterns for Fe_2O_3 and K/Fe_2O_3 shows very clearly that the proportion of carbide phases in K/Fe_2O_3 is greater than that in Fe_2O_3. In contrast to the unreduced catalysts, the diffraction pattern for reduced Fe_2O_3 shows no evidence for Fe_3O_4. The majority of the peaks are attributable to χ-carbide, but small amounts of ε'-carbide and α-Fe are also observed.

DISCUSSION

Nature of the Active Catalyst

The activity versus reaction time data presented in Figs. 2 and 3 clearly demon-

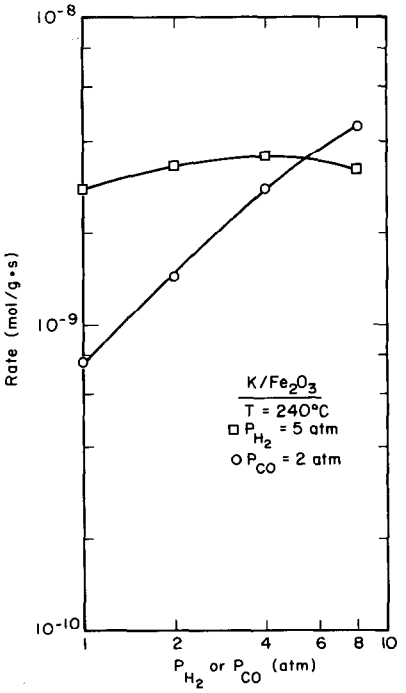

FIG. 16. Rate of acetaldehyde production as a function of reactant partial pressures.

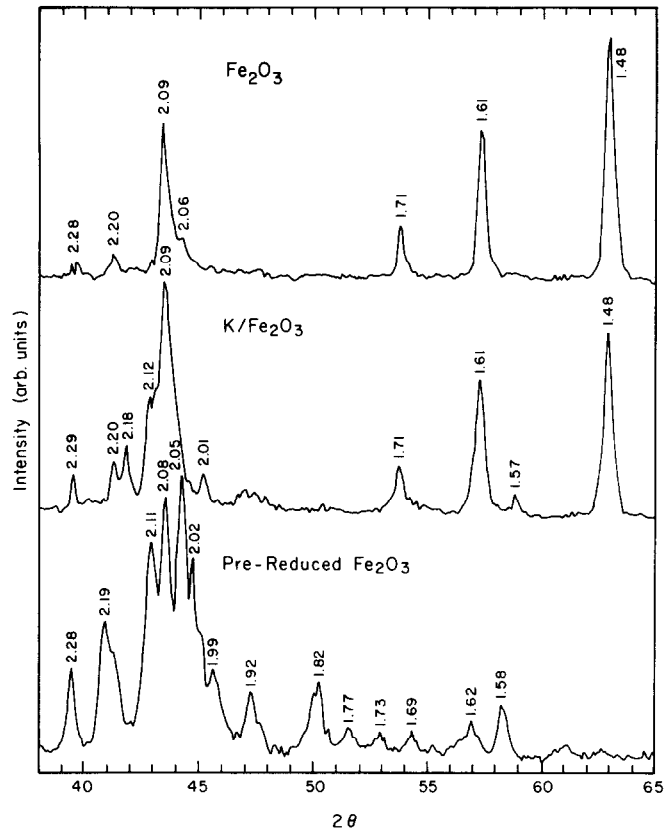

FIG. 17. X-Ray diffraction patterns for used Fe_2O_3, K/Fe_2O_3, and prereduced Fe_2O_3 catalysts.

strate that unreduced Fe_2O_3 and K/Fe_2O_3 are inactive for Fischer–Tropsch synthesis. On the other hand, the results in Fig. 1 show that reduced Fe_2O_3 exhibits immediate activity. The reduction of Fe_2O_3 is known to proceed rapidly to Fe_3O_4 and more slowly to Fe (*1–3*). Wustite, FeO, is not produced for reduction temperatures below 570°C (*25–28*). This suggests that the rapid production of CO_2 during the first 5 to 10 h of exposure to syngas is due to the reduction of Fe_2O_3 to Fe_3O_4. The amounts of CO_2 released during the induction period seen in Figs. 2 and 3 are in very good agreement with this interpretation. The slow rise in synthesis activity following the induction period suggests further that Fe_3O_4 is also inactive and that the activity arises from a reduction of Fe_3O_4 to α-Fe. Once formed, small particles of α-Fe will readily carburize to form ε'- and χ-carbides (*10*). This would explain the absence of large amounts of α-Fe in the X-ray diffraction patterns of the used catalysts.

The similarity of the product distributions and kinetics of the Fischer–Tropsch synthesis over reduced and unreduced Fe_2O_3, together with the absence of any evidence for Fe_3O_4 in the X-ray diffraction spectrum of reduced Fe_2O_3 taken after extensive use, further supports the contention that Fe_3O_4 is inactive for Fischer–Tropsch synthesis. This conclusion contradicts that reached by Reymond *et al.* (*12–14*). These authors interpreted the absence of a delay in the onset of synthesis activity upon contact of unreduced Fe_2O_3 with syngas to suggest that Fe_3O_4 is an active component of the catalyst. This evidence cannot, however, be regarded as conclusive proof for

TABLE 2

Assignment of X-Ray Diffraction Peaks for Used Catalysts[a]

d/n (Å)			Assignment[b]
Reduced Fe_2O_3	Unreduced Fe_2O_3	Unreduced K/Fe_2O_3	
2.28	2.28	2.29	χ-$Fe_{2.2}C$
2.20	2.20	2.20	χ-$Fe_{2.2}C$
2.19	—	2.18	χ-$Fe_{2.2}C$
2.11	—	2.12	ε'-Fe_5C_2
—	2.09	2.09	Fe_3O_4
2.08	—	—	χ-$Fe_{2.2}C$
2.05	2.06	2.06	χ-$Fe_{2.2}C$
2.02	—	—	α-Fe
2.01	—	2.01	χ-$Fe_{2.2}C$
1.99	—	—	χ-$Fe_{2.2}C$
1.92	—	—	χ-$Fe_{2.2}C$
1.82	—	—	χ-$Fe_{2.2}C$
1.77	—	—	χ-$Fe_{2.2}C$
1.73	—	—	. . .
—	1.71	1.71	Fe_3O_4
1.69	—	—	. . .
1.62	1.61	1.61	Fe_3O_4
1.58	1.57	—	χ-$Fe_{2.2}C$
—	1.48	1.48	Fe_3O_4

[a] Catalysts were characterized after approximately 10 days of continuous use.

[b] Assignments for χ-$Fe_{2.2}C$ are based on Ref. (*24*), for ε'-Fe_5C_2 on Ref. (*11*), for α-Fe on Ref. (*23*), and for Fe_3O_4 on Ref. (*23*).

the activity of Fe_3O_4. Reymond *et al.* (*12–14*) carried out their experiments with syngas having an H_2/CO ratio of 9. For such a high H_2/CO ratio, the reduction of Fe_2O_3 to Fe_3O_4 will proceed very rapidly, with the consequence that the delay in the onset of synthesis activity will be eliminated. In view of this, we would interpret the slow rise in synthesis activity with time observed by Reymond *et al.* (*12–14*) as being due to the progressive reduction of Fe_3O_4 to form α-Fe or a mixture of α-Fe and χ-$Fe_{2.2}C$.

The question of whether iron or iron carbide is the active phase for Fischer–Tropsch synthesis cannot be resolved by the present results. Raupp and Delgass (*10*) have reported that the rise in activity of supported iron catalysts parallels the increasing carbide of the content of the catalyst. Bonzel *et al.* (*4–7*) and Dwyer and Hardenbergh (*9*) have shown similar results for polycrystalline iron. This might suggest that iron carbide is required to obtain a high synthesis activity. On the other hand, Niemantsverdriet *et al.* (*11, 29*) have proposed that iron carbide may not be essential for hydrocarbon synthesis, and that the parallel rise in the rate of hydrocarbon formation with increasing carbide content of the catalyst is due to the fact that hydrocarbons and carbides are formed from the progressive accumulation of a common precursor.

As shown in Fig. 1, reduction of Fe_2O_3 results in a high initial activity. This activity level cannot be maintained, though, and declines fairly rapidly with time. Similar observations have been made in other studies with reduced iron catalysts and it has been suggested that the loss in activity is due primarily to the accumulation of unreactive carbon (*2*). By contrast to the performance of reduced Fe_2O_3, unreduced Fe_2O_3 shows no evidence of deactivation, even after continuous use for 10 days or more. This difference in the behavior of reduced and unreduced Fe_2O_3 may be a function of the size and number of Fe or χ-$Fe_{2.2}C$ crystallites present in the catalyst. The X-ray diffraction patterns presented in Fig. 17 indicate that after 10 days of use, the reduced Fe_2O_3 catalyst contains considerably more χ-$Fe_{2.2}C$ than the unreduced catalyst; however, the activity of the unreduced catalyst is higher than that of the reduced catalyst. These observations suggest that the crystallites of χ-$Fe_{2.2}C$ in the unreduced catalyst are much smaller than those formed in the reduced catalyst. The small size of the carbide crystallites might also be responsible for the lower rate of deactivation of the unreduced catalyst.

Product Distribution

The Anderson–Schulz–Flory plots presented in Figs. 4 and 7 show that the distribution of C_1–C_{15} products for Fe_2O_3 and K/

Fe_2O_3 can be described by two straight lines. The value of α for the C_8–C_{15} products is consistently greater than that for the C_1–C_7 products. Similar breaks in the distribution have been observed for fused iron (*30–32*), precipitated iron (*33, 34*) and iron alloy (*35*) catalysts. The origin of the break is not clearly established. Konig and Gaube (*33*) and Huff and Satterfield (*34*) have proposed that the two branches observed with potassium-promoted iron catalysts are due to synthesis over two groups of active sites differing in their level of promotion. This interpretation may not be the only one, though, since Huff and Satterfield (*34*) have shown more recently that some unpromoted iron catalysts also produce Anderson–Schulz–Flory plots consisting of two branches. It is conceivable that in the absence of a promoter, nonuniformities in the structure and/or composition of the active phase is responsible for the appearance of two branches in product distribution plots.

In agreement with many previous studies (see, for example, Refs. (*1–3*)), the present results confirm that olefins are produced as a primary product of Fischer–Tropsch synthesis over iron catalysts. Paraffins are also formed directly but to a much lesser degree than olefins. The high proportion of paraffinic hydrocarbons observed using Fe_2O_3 arises from the secondary hydrogenation of olefins. This is well illustrated by the sensitivity of the olefin content to variations in syngas flow rate. Since olefin hydrogenation requires the presence of adsorbed hydrogen, it is not surprising that the paraffin content of the products formed over Fe_2O_3 increases with increasing H_2 or decreasing CO partial pressure. Potassium promotion enhances the adsorption of CO and decreases the adsorption of H_2 (*35–37*). Consistent with this, the extent of olefin hydrogenation is suppressed.

The conversion of primary olefins to secondary olefins is also a secondary process. Here, too, adsorbed hydrogen is required. As demonstrated by the results in Fig. 6, the extent of internal olefins formed increases with increasing H_2 partial pressure. Potassium promotion of Fe_2O_3 has the opposite effect, greatly suppressing olefin isomerization.

The similarity in the response of olefin hydrogenation and isomerization to potassium promotion and to the partial pressures of H_2 and CO suggest that a common set of intermediates are involved. A plausible reaction scheme is illustrated in Fig. 18a. A primary olefin is adsorbed in the vicinity of an adsorbed hydrogen atom. Further addition of a hydrogen atom to the adsorbed alkyl species leads to formation of a normal paraffin molecule. On the other hand, hydrogen elimination from the γ-carbon of the branched alkyl species produces a β-olefin molecule.

Branched olefins were not observed over Fe_2O_3 but were over K/Fe_2O_3. The insensitivity of the proportion of branched products to syngas flow rate suggests that these products are formed via primary processes. A possible scheme is shown in Fig. 18b. The formation of linear alkyl species is taken to proceed via the addition of adsorbed methylene with adsorbed alkyl groups. Chain branching might occur by the loss of an α-hydrogen from the alkyl group to produce an alkylidene, followed by methylene addition to produce a metallocylic species. Depending upon whether hydrogen addition in the next step is to the α- or β-carbon atom, either a linear or a branched alkyl species will result. Further methylene addition to the branched alkyl would produce a branched olefin or paraffin. Since the formation of the alkylidene is impeded by the presence of adsorbed hydrogen, a reduction in the surface concentration of this species would be expected to enhance chain branching. This is probably the reason why chain branching occurs more readily over K/Fe_2O_3 than Fe_2O_3.

Figure 9 shows that the carbon number distribution for C_2^+ aldehydes produced over K/Fe_2O_3 is quite similar to that of hydrocarbons. This suggests that aldehydes and olefins are produced from a common

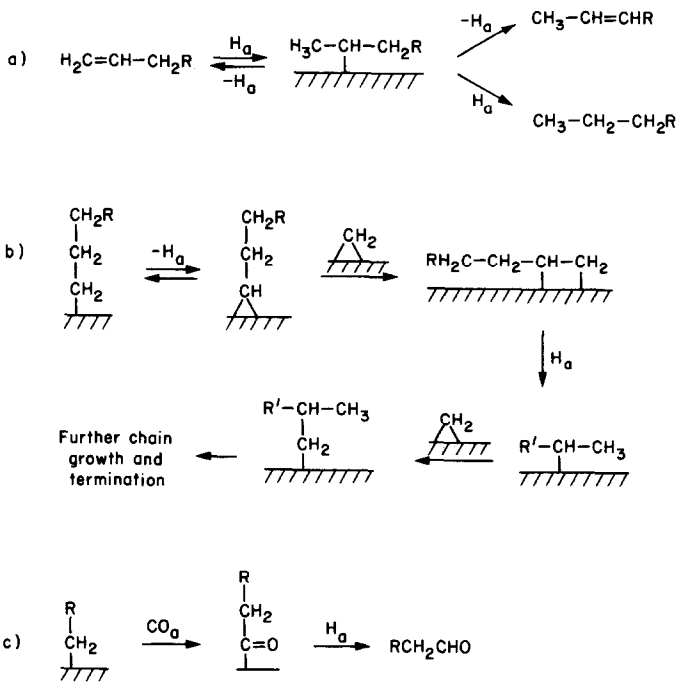

FIG. 18. Reaction pathways for: (a) isomerization of α- to β-olefins; (b) formation of branched olefins and paraffins; and (c) formation of aldehydes.

precursor. An illustration of how aldehydes might be formed is given in Fig. 18c. The process begins with insertion of a CO molecule into the metal–carbon bond of an alkyl group, to produce an acyl group. Reductive elimination of the acyl produces the corresponding aldehyde. The fact that potassium promotion is required to achieve a high proportion of aldehydes suggests that potassium may assist in the carbonylation step. One possibility is that potassium ions form a Lewis acid-base adduct with the oxygen end of adsorbed CO molecules. This would have the effect of tipping the axis of the CO molecule toward the surface and weakening the C–O bond. Studies with homogeneous catalysts have shown that CO insertion into metal–alkyl bonds is enhanced by adducts of the type described above (*38, 39*).

Kinetics

The product distribution presented in Figs. 4 and 7 show that for $n = 1$ to $n = 7$ the rates of product formation fall along a staight line. The equation for this line is

$$R_{C_n} = R_1\alpha^{n-1}, \qquad (1)$$

where R_{C_n} is the molar rate of production of hydrocarbons with n carbon atoms and R_1 is the apparent rate of synthesis for $n = 1$ but does not necessarily represent the rate of methane formation. The dependence of R_{C_n} on temperature and H_2 and CO partial pressures can now be expressed through R_1 and α.

From its definition, we can relate α to the ratio of the rates of chain propagation, r_p, and chain termination, r_t. Thus

$$\frac{1-\alpha}{\alpha} = \frac{r_p}{r_t}. \qquad (2)$$

We presume that the right-hand side of Eq. (3) will be a function of temperature and the partial pressures of H_2 and CO. Figure 19 shows that the experimentally observed values of α produce a straight line when $(1 - \alpha)/\alpha$ is plotted versus P_{H_2}/P_{CO}. For Fe_2O_3, the equation of the line is

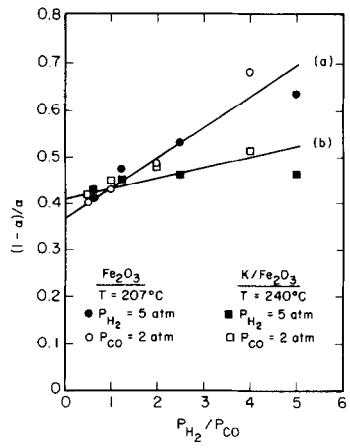

FIG. 19. Empirical correlation between α and reactant partial pressures.

$$\frac{(1-\alpha)}{\alpha} = 0.367 + 0.065\, P_{H_2}/P_{CO} \quad \text{for } T = 207°C \quad (3)$$

and for K/Fe_2O_3 it is

$$\frac{(1-\alpha)}{\alpha} = 0.410 + 0.024\, P_{H_2}/P_{CO} \quad \text{for } T = 240°C \quad (4)$$

R_1 can be represented in the form of a power-law rate expression

$$R_1 = k_1 P_{H_2}^{x} P_{CO}^{y}, \quad (5)$$

where k_1 is the effective rate coefficient, and x and y are the exponents on P_{H_2} and P_{CO}, respectively. The values of k_1, x, and y are found by fitting R_{C_n}/α^{n-1} to Eq. (5). The resulting expression for Fe_2O_3 is

$$R_1 = 3.58 \times 10^{-9}\, P_{H_2}^{1.07}\, P_{CO}^{-0.51} \frac{\text{mol}}{\text{g} \cdot \text{s}} \quad \text{for } 207°C \quad (6)$$

and for K/Fe_2O_3

$$R_1 = 4.66 \times 10^{-9}\, P_{H_2}^{0.91}\, P_{CO}^{-0.18} \frac{\text{mol}}{\text{g} \cdot \text{s}} \quad \text{for } 240°C. \quad (7)$$

The kinetics of hydrocarbon synthesis over Fe_2O_3 can be obtained by substitution of Eqs. (3) and (7) into Eq. (1). The representation of the data in this fashion is shown by the solid lines in Figs. 10 and 11 for $n \geq 3$. The curvature seen in the lines is a direct result of the dependence of α on the reactant partial pressures and the dependence of R_{C_n} on α^{n-1}. Similar reasoning can be used to explain the curvature of the Arrhenius plot shown in Fig. 12.

Since the dependence of α on H_2 and CO partial pressures for K/Fe_2O_3 is much weaker than for Fe_2O_3, the kinetics for hydrocarbon synthesis over K/Fe_2O_3 is dominated by the power-law dependence of R_1 (Eq. (7)). This explains why the lines shown in Figs. 12 and 13 are straight and show little change in slope with n.

CONCLUSIONS

The products of Fischer–Tropsch synthesis over reduced and unreduced Fe_2O_3 are similar. Methane and terminal olefins are formed directly from CO and H_2, while C_2^+ normal paraffins and internal olefins are produced by secondary reaction of the C_2^+ terminal olefins. No branched products are formed over either catalyst. Methanol is the principal oxygenated product observed. The carbon number distribution of hydrocarbon products can be described by two Anderson–Schulz–Flory distributions differing in the value of α. The magnitude of α for C_1–C_7 products is always less than that for C_8–C_{15} products. The values of α increase with increasing CO partial pressure and decreasing H_2 partial pressure and temperature. The conversion of terminal olefins to internal olefins and paraffins increases with increasing temperature and H_2 partial pressure, and with decreasing CO partial pressure.

Promotion of Fe_2O_3 with potassium decreases the synthesis activity of unreduced Fe_2O_3 but results in an increase in the values of α associated with the distribution of hydrocarbon products. Potassium promotion also causes a nearly complete suppression of C_2^+ olefin isomerization and hydrogenation, and methanol formation. Noticeable quantities (10–20%) of branched products and C_2^+ aldehydes are formed over

K/Fe_2O_3, neither of which is observed over unpromoted Fe_2O_3. The latter two sets of products are produced by primary processes.

X-Ray diffraction analysis of used catalysts reveals that reduced Fe_2O_3 consists primarily of χ-$Fe_{2.2}C$ with smaller amounts of α-Fe, while unreduced Fe_2O_3 and K/Fe_2O_3 consist of χ-$Fe_{2.2}C$ supported on Fe_3O_4. The behavior of the unreduced catalysts with time under reaction conditions indicates that neither Fe_2O_3 nor Fe_3O_4 are active for hydrocarbon synthesis and that the active components are α-Fe and/or χ-$Fe_{2.2}C$. The superior maintenance of synthesis activity of the unreduced catalysts is believed to be due to the presence of very small crystallites of the active phases.

ACKNOWLEDGMENTS

This work was jointly supported by the Director, Office of Energy Research, Office of Basic Energy Sciences, Chemical Science Division and the Assistant Secretary for Fossil Energy, Office of Coal Research, Liquefaction Division of the U.S. Department of Energy under Contract DE-AC03-76SF00098 through the Pittsburgh Energy Technology Center, Pittsburgh, Pa.

REFERENCES

1. Storch, H. H., Golumbic, N., and Anderson, R. B., "The Fischer–Tropsch and Related Syntheses." Wiley, New York, 1951.
2. Dry, M. E., *in* "Catalysis: Science and Technology" (Boudart, M., and Anderson, J. R., Eds.), Vol. 1. Springer-Verlag, New York, 1981.
3. Anderson, R. B., "The Fischer–Tropsch Synthesis." Academic Press, New York, 1984.
4. Krebs, H. J., Bonzel, H. P., and Gafner, G., *Surf. Sci.* **88,** 269 (1979).
5. Bonzel, H. P., and Krebs, H. J., *Surf. Sci.* **91,** 499 (1980).
6. Bonzel, H. P., and Krebs, H. J., *Surf. Sci.* **117,** 639 (1982).
7. Krebs, H. J., Bonzel, H. P., Sebwarting, W., and Gafner, G., *J. Catal.* **63,** 226 (1980).
8. Dwyer, D. J., and Somorjai, G. A., *J. Catal.* **52,** 291 (1978).
9. Dwyer, D. J., and Hardenbergh, H., *J. Catal.* **87,** 66 (1984).
10. Raupp, G. B., and Delgass, W. N., *J. Catal.* **58,** 348, 361 (1979).
11. Niemantsverdriet, J. W., van der Kraan, A. M., van Dijk, W. L., and van der Baan, H. S., *J. Phys. Chem.* **84,** 3363 (1980).
12. Reymond, J. P., Mériaudeau, P., and Teichner, S. J., *J. Catal.* **75,** 39 (1982).
13. Blanchard, F., Reymond, J. P., Pommier, B., and Teichner, S. J., *J. Mol. Catal.* **17,** 171 (1982).
14. Reymond, J. P., Pommier, B., Mériaudeau, P., and Teichner, S. J., *Bull. Soc. Chim. Fr.* **1,** 173 (1981).
15. Dictor, R. A., and Bell, A. T., *Ind. Eng. Chem. Fundam.* **2,** 252 (1984).
16. Dictor, R. A., and Bell, A. T., *Ind. Eng. Chem. Proc. Des. Dev.* **22,** 678 (1983).
17. Schulz, H., Rösch, S., and Gökcebay, H., *in* "Proceedings, International Conference on Coal Science," Düsseldorf, Sept. 1981.
18. Schulz, H., and Gökcebay, H., *in* Prepr. 9th Conf. Catal. Org. React.," Charleston, S.C., April 1982.
19. Schulz, H., and Zein El Deen, A., *Fuel Process. Technol.* **1,** 45 (1977).
20. Biloen, P., Helle, J. N., and Sachtler, W. M. H., *J. Catal.* **58,** 95 (1979).
21. Satterfield, C. N., Huff, Jr., G. A., and Summerhayes, R., *J. Catal.* **80,** 486 (1983).
22. Cannella, W. J., and Bell, A. T., unpublished results.
23. National Bureau of Standards, Monograph 25, Sect. 5, 31 (1967).
24. Jack, K. H., *Proc. R. Soc. London Ser. A* **195,** 56 (1948).
25. Viswanath, R. P., Viswanathan, B., and Sastri, M. V. C., *Trans. Jpn. Inst. Met.* **18,** 149 (1977).
26. Ramachandran, N., and Chakrabarty, D. K., *Proc. Indian Acad. Sci.* **89,** 533 (1980).
27. Bessieres, J., Bessieres, A., and Heizman, J. J., *Int. J. Hydrogen Energy* **5,** 585 (1980).
28. Darken, C. S., and Gurry, R. W., *J. Amer. Chem. Soc.* **68,** 799 (1946).
29. Niemantsverdriet, J. W., and van der Kraan, A. M., and van Loef, J. J., *J. Catal.* **72,** 385 (1981).
30. Cannella, W., and Bell, A. T., unpublished results.
31. Weitkamp, A. W., Seelig, H. S., Bowman, N. J., and Cady, W. E., *Ind. Eng. Chem.* **45,** 343 (1953).
32. Huff, G. A., Jr., and Satterfield, C. N., submitted for publication.
33. Konig, L., and Gaube, J., *Chem.-Ing.-Tech.* **55,** 14 (1983).
34. Huff, G. A., Jr., and Satterfield, C. N., *J. Catal.* **85,** 370 (1984).
35. Dry, M. E., Shingles, T., Boshoff, L. J., and Oosthuizen, G. J., *J. Catal.* **15,** 190 (1969).
36. Benziger, J., and Madix, R. J., *Surf. Sci.* **94,** 119 (1980).
37. Arakawa, H., and Bell, A. T., *I&EC Proc. Des. Dev.* **22,** 97 (1983).
38. Butts, S. S., Strauss, S. H., Holt, E. M., Stimson, R. E., Alcock, N. W., and Shiver, D. F., *J. Amer. Chem. Soc.* **102,** 6093 (1980).
39. Correa, F., Nakamura, R., Steinson, R. E., Burwell, R. L., Jr., and Shiver, D. F., *J. Amer. Chem. Soc.* **102,** 5112 (1980).